Available online at www.sciencedirect.com

ScienceDirect

Ceramics International 41 (2015) 2806–2812

CERAMICS INTERNATIONAL

www.elsevier.com/locate/ceramint

One pot solution combustion synthesis of highly mesoporous hematite for photocatalysis

Zhiqin Cao[a,b], Mingli Qin[a,*], Baorui Jia[a], Yueru Gu[a], Pengqi Chen[a], Alex A. Volinsky[c], Xuanhui Qu[a]

[a]School of Materials Science and Engineering, University of Science and Technology Beijing, Beijing 100083, China
[b]School of Resources and Environmental Engineering, Pan Zhihua University, Pan Zhihua 617000, China
[c]School of Resources and Environmental Engineering, Pan Zhihua University , Pan Zhihua 617000, China

Received 17 September 2014; received in revised form 17 October 2014; accepted 17 October 2014
Available online 24 October 2014

Abstract

Iron oxides were synthesized by solution combustion synthesis using glycine (fuel) and ferric nitrate (oxidizer) as raw materials. The effects of the fuel to oxidizer ratio, ϕ, on the combustion behavior, phase, morphology and surface area of the products were systematically studied. Pure hematite was synthesized directly by the combustion of the precursors under fuel-lean conditions in one step without further heat treatment, simply by selecting a proper fuel to oxidizer ratio, ϕ. The hematite has a highly mesoporous structure with specific surface area of 103 $m^2 g^{-1}$ and an average size of about 20 nm, which was obtained at $\phi = 0.3$. The hematite displays a continuous absorption band in the visible region. The photocatalytic activity of the hematite was evaluated by degrading the methylene blue pollutant in water at ambient temperature. The synthesized mesoporous hematite is a promising visible light photocatalysts for organics decomposition.

Keywords: hematite; mesoporous; solution combustion synthesis; photocatalytic

1. Introduction

Semiconductor catalysts have been widely applied as photocatalyst in solar cells, water splitting, lithium ion batteries, gas sensors, and waste water treatment [1–5]. Hematite (α-Fe_2O_3) has a band gap of 1.9–2.2 eV, and could be a potential semiconductor catalyst of visible light driving [6]. Moreover, compared with other narrow band gap semiconductors (CdS, Bi_2WO_6, $Zn_2In_2S_4$), α-Fe_2O_3 has excellent environmental compatibility and lower cost [7–10]. Due to these attractive characteristics, many efforts have been made to synthesize α-Fe_2O_3 photocatalysts, e.g. hydrothermal, atomic layer deposition, ultrasonic spray pyrolysis and low temperature reflux condensation methods [11–14]. These results indicate that mesoporous nanocrystalline α-Fe_2O_3 displays excellent catalytic activity and the mesoporous materials have lots of advantages in photocatalytic applications [15,16] due to the large surface area generated by mesopores, high surface-to-volume ratio, particular morphology, well-defined topology, and pore diameter. Hence, it is of significant interest to develop a simple, inexpensive method to prepare mesoporous nanocrystalline α-Fe_2O_3 with high specific surface area.

Solution combustion synthesis (SCS) is a well-known method for the preparation of nanocrystalline oxides [17–21]. In this method, oxidizer (usually in the form of nitrates) is dissolved in water along with fuel (usually urea, glycine citrate, and so on). The solution is then heated in an open container on a hotplate, evaporating water and, upon reaching a critical temperature, causing the decomposition of the nitrate, which ignites the fuel. The advantages of this synthesis technique include low external heating requirements (as the fuel provides energy for product formation), precursor mixing at the molecular level, ensured by the reagent dissolution in water, and product with high specific surface area synthesized due to a large volume of gases liberated during the combustion

*Corresponding author. Tel.: +86 10 82377286; fax: +86 10 62334311.
E-mail address: qinml@mater.ustb.edu.cn (M. Qin).

http://dx.doi.org/10.1016/j.ceramint.2014.10.100
0272-8842/

reaction. This method has been regarded as effective and economic due to its energy saving, convenient processing, simple experimental set up, significant time savings and high purity products. Because of these advantages, various iron oxides have been prepared by the SCS. For example, Toniolo et al. [22] have reported synthesis of α-Fe_2O_3/Fe_3O_4 composite by combustion synthesis with ferric nitrate-urea precursor. Deshpande et al. [23] prepared ferrimagnetic Fe_3O_4 powders by conducting the combustion reaction between ferric nitrate and hydrazine, or glycine in argon atmosphere. Hu et al. [24] have reported the auto-combustion reaction of the citrate-ferric nitrate precursor, which yielded α-Fe_2O_3 powder.

In this work, mesoporous nanocrystalline α-Fe_2O_3 was synthesized from the combustion reaction of glycine (fuel) and ferric nitrate (oxidizer). Effects of fuel to oxidizer ratio on the combustion reaction, the phase, morphology and specific surface areas (SSA) of the products were investigated in detail. The photocatalytic experiments indicated that the synthesized α-Fe_2O_3 is a promising candidate for the catalytic decomposition of organics.

2. Experimental

2.1. Synthesis

The products were prepared by solution combustion synthesis using ferric nitrate [$Fe(NO_3)_3 \cdot 9H_2O$] as the oxidizer and glycine [NH_2CH_2COOH] as the fuel. Analytical reagent grade chemicals were purchased commercially. As a typical sample preparation procedure, $Fe(NO_3)_3 \cdot 9H_2O$ and NH_2CH_2COOH were dissolved in 150 mL deionized water under stirring to obtain a homogeneous solution. The mixture was filled in a 500 mL glass, and heated in air in a temperature-controlled electrical furnace. As heating continued, the solution evaporated and formed a gelatinous mass. It took several minutes to form this gelatinous mass. Upon further heating, the resultant mass suddenly swelled, accompanied by the release of lots of gases. The whole process of gel swelling and combustion appeared to undergo a self-propagating and non-explosive exothermic reaction, which took short time, resulting in fragile and foamy products.

2.2. Characterization

The products were analyzed by X-ray diffraction (XRD) using Cu-K_α ($\lambda = 0.1542$ nm) radiation (Rigaku, D/max-RB12). The morphology of the prepared products was studied by scanning electron microscopy (SEM, JSM-5600) and transmission electron microscopy (TEM, Tecnai G2 F30 S-TWIN). The X-ray photoelectron spectroscopy (XPS) analysis was carried out using AXIS Ultra DLD spectrometer equipped with an Al Kα X-ray source and electrostatic hemispherical electron analyzer. The SSA was estimated by applying the Brunauer-Emmett-Teller (BET) method by using an Automated Surface Area & Pore Size Analyzer (QUADRASORB SI-MP, Quantachrome Instruments, Boynton Beach, FL). Ultraviolet (UV)-visible diffused reflectance spectra of the product was obtained using a UV-visible spectrophotometer.

2.3. Photocatalytic performance under visible light irradiation

The photocatalytic activity was evaluated according to the decomposition of methylene blue (MB) as a model contaminant under visible light irradiation. Experiments were performed at ambient temperature as follows. 0.05 g samples as the photocatalysts were added to 100 mL of the MB solution with 20 mg L^{-1} concentration in a quartz vessel. Prior to illuminating the sample, the reaction mixture was stirred for 20 min in the dark to obtain a good dispersion and permit equilibration of the adsorption-desorption processes between the catalyst surface and MB. After adding 1 mL of a 30% hydrogen peroxide (H_2O_2) solution as an oxidant to the above reaction mixture, the lamp was turned on. A commercial 250 W halogen spotlight (the spectrum below 400 nm was removed using a cutoff filter) was used for the visible light illumination. The absorption of the MB aqueous solution was monitored spectrophotometrically at $\lambda_{max} = 664$ nm during the photodegradation process.

3. Results and discussion

3.1. Synthesis and characterization of the products

In solution combustion synthesis, the fuel to oxidizer ratio has been previously shown to alter the combustion behavior, oxidation state, morphology and SSA of the products [25–30]. Therefore, the effect of fuel (glycine) to oxidizer (ferric nitrate) ratio on the formation of products was investigated first. The reaction can be presented as follows:

$$Fe(NO_3)_3 + \frac{5}{3}\phi\, C_2H_5NO_2 + \frac{15}{4}(\phi - 1)O_2 \rightarrow \frac{1}{2}Fe_2O_3 + \frac{10}{3}\phi\, CO_2 + \frac{25}{6}\phi\, H_2O + \left(\frac{5}{3}\phi + 3\right)/2N_2 \quad (1)$$

Here, the fuel to oxidizer ratio, denoted by ϕ, represents a tunable parameter, where ϕ=1 (stoichiometric) means that the initial mixture does not require atmospheric oxygen for complete fuel oxidation, while $\phi > 1$ (or < 1) implies fuel-rich (or lean) conditions. Fig. 1 shows the XRD patterns of the products with different ϕ. For the products with $\phi = 0.1$, although the diffraction peaks identified for the planes of the α-Fe_2O_3 crystalline structure can be detected, the α-Fe_2O_3 is not well crystallized. As the ϕ increases, the heat generated by the combustion reaction increases and the crystallization of the products is gradually perfected. For products with ϕ of 0.2, 0.3, 0.6, it is evident that the obvious diffraction peaks identified for the planes of the pure α-Fe_2O_3 crystalline structure can be clearly detected. When ϕ is increasing to 1 and 1.2, γ-Fe_2O_3 diffraction peaks can also be observed, indicating that the products are a mixture of α-Fe_2O_3 and γ-Fe_2O_3. These results indicate that ϕ has a great influence on the phase of the products, and pure crystalline α-Fe_2O_3 can be prepared by the combustion of the precursors under fuel lean conditions in one step without further heat treatment, simply by selecting a proper fuel to oxidizer ratio, ϕ.

Deshpande et al. [26] have conducted a systematic study of the ϕ effect on the phase of products by using glycine as fuel

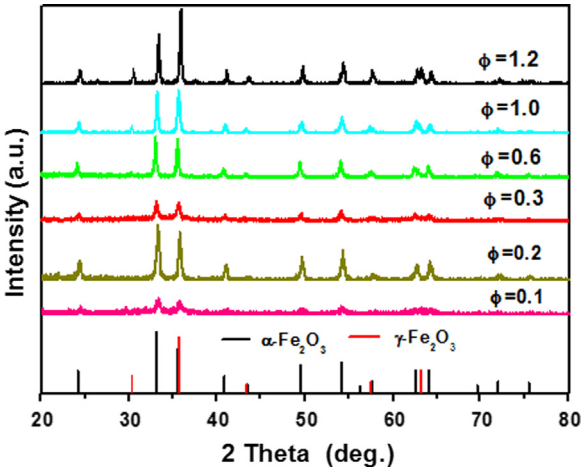

Fig. 1. The XRD patterns of the products obtained by the solution combustion synthesis with different ϕ.

and ferric nitrate as oxidizer. Their research focused on the fuel-rich region (ϕ ranging from 1 to 3). They found that the combustion product with $\phi=1$ was also a mixture of α-Fe_2O_3 and γ-Fe_2O_3, while the products obtained with $\phi>1$ had a well-defined crystalline structure of pure α-Fe_2O_3. This research shows that pure crystalline α-Fe_2O_3 can also be prepared under the fuel-lean conditions ($\phi<1$). This result is very interesting because it means that little amounts of fuel can be used to synthesize pure α-Fe_2O_3 by the solution combustion method, and the combustion process could be easily controlled. The mechanism of the ϕ effect on the phase of the products is under investigation in this research.

Fig. 2 shows SEM images of the products with different ϕ. For $\phi=0.1$, the products are composed of agglomerated particles (Fig. 2a). As the amount of fuel is increased, the morphology of the combustion products has changed. For $\phi=0.2$ and 0.3 (Fig. 2b and c), the products are composed of

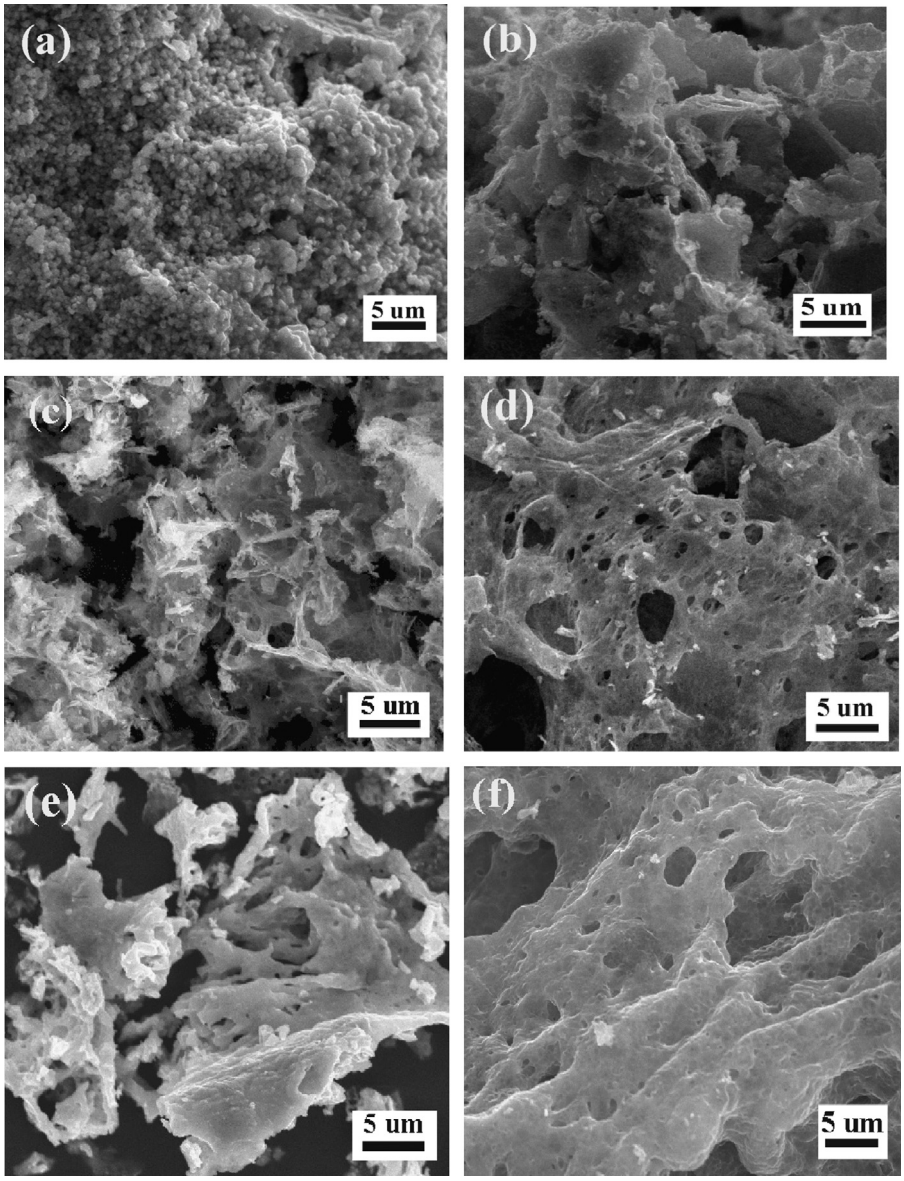

Fig. 2. SEM images of the products obtained by the solution combustion synthesis with different ϕ: (a) 0.1; (b) 0.2; (c) 0.3; (d) 0.6; (e) 1; (f) 1.2.

thin flakes. As ϕ increased from 0.6, to 1 and 1.2, the morphology of the as-prepared products changed from sponge, to bulk (Fig. 2d, e and f). Nitrogen adsorption/desorption isotherms were measured to determine the SSA of the products. The SSA of the products for $\phi=0.1$, 0.2, 0.3, 0.6, 1.0 and 1.2 are 10 m^2 g^{-1}, 32 m^2 g^{-1}, 103 m^2 g^{-1}, 32 m^2 g^{-1}, 4 m^2 g^{-1} and 10 m^2 g^{-1} respectively, shown in Fig. 3). These results show that the morphology and specific surface of the synthesized products are sensitive to the ϕ parameter changes. In solution combustion process, the amount of fuel (or the ratio of fuel to oxidizer, ϕ) has a great influence on the amount of energy and the volume of gases liberated by the combustion reaction [31,32].As the amount of fuel increases, the amount of energy and the volume of gases increase. The larger volume of gases can increase SSA of the products and the SSA reaches the maximum of 103 m^2 g^{-1} at ϕ=0.3. With further ϕ increase, although the volume of the gases increases, the energy also increases. According to the theory of chemical propellants, the reaction releases the maximum energy at stoichiometric composition (ϕ=1). Under the fuel-rich regime ($\phi > 1$), molecular oxygen is required to obtain complete combustion. The higher energy released during the reaction leads to a swift rise in temperature in a narrow timeframe. The enhancement in the combustion temperature and time during the reaction renders the products to display similar behavior to sintering. The products are agglomerated as bulk and the SSA is decreased.

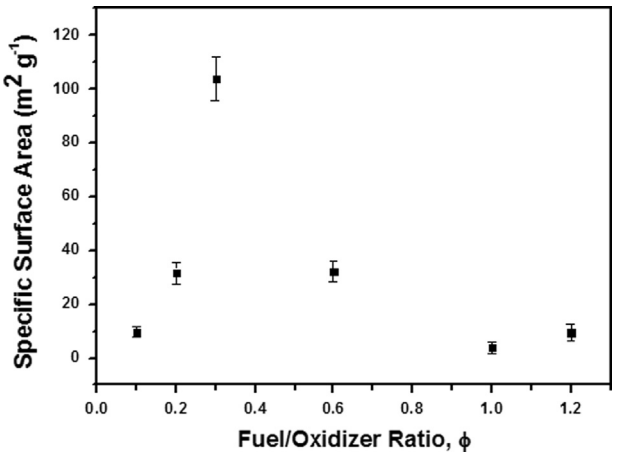

Fig. 3. Surface area dependence for the fuel/oxidizer ratio, ϕ.

The products with ϕ=0.3 were further investigated by XPS, TEM and BET methods, and the results are shown in Fig. 4. Fig. 4a and b show the XPS spectra of the products. Fig. 4a depicts the XPS spectra of Fe 2p. The Fe 2p spectra indicate the existence of doublet Fe $2p^{3/2}$ and Fe $2p^{1/2}$, with binding energies around 710 eV and 723 eV, respectively. The Fe $2p^{3/2}$ peak is also associated with a satellite peak located approximately 7 eV

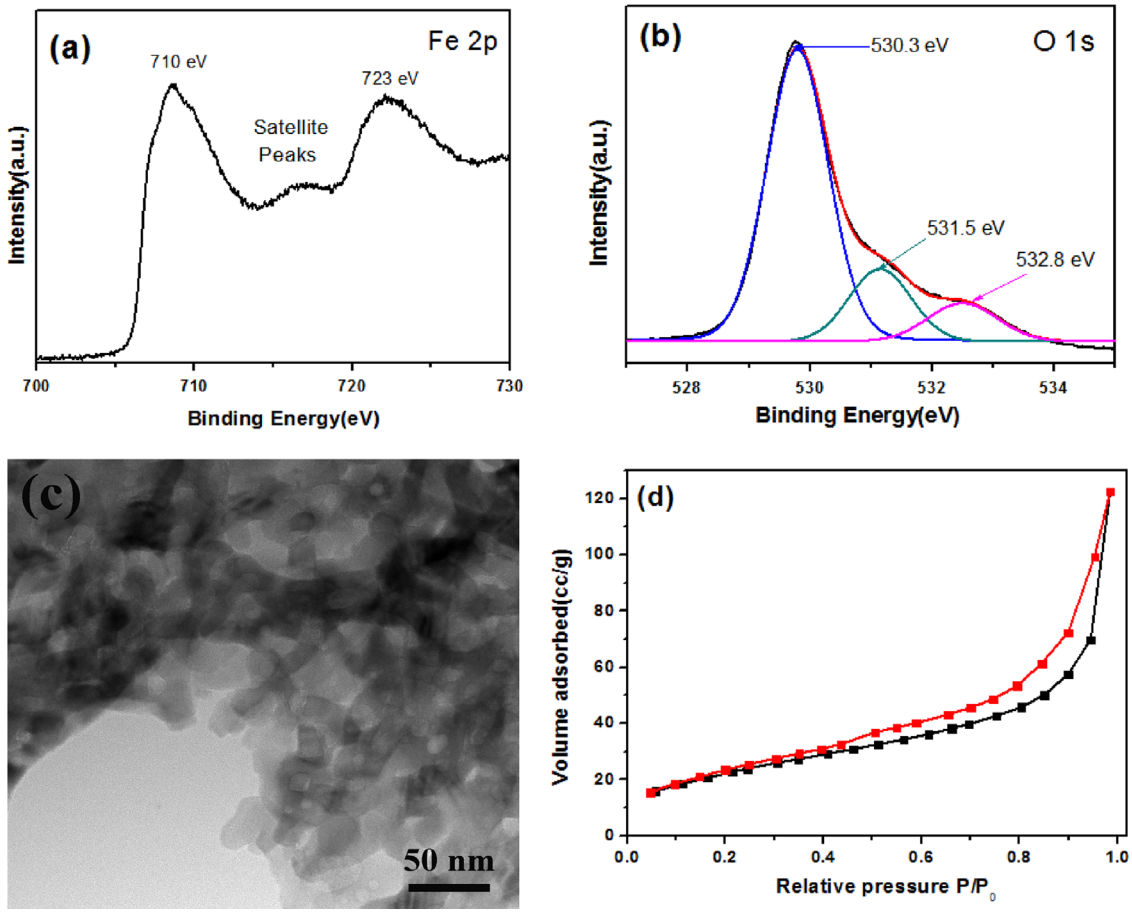

Fig. 4. Structural characterization of the sample with ϕ=0.3: (a) and (b) XPS spectra; (c) TEM image; (d) Nitrogen adsorption/desorption isotherms.

higher than the main peak, which is characteristic of hematite [33]. The corresponding satellite peak noted at 717 eV is a result of charge transfer screening. It can be attributed solely to the presence of Fe^{3+} ions of α-Fe_2O_3. A high-resolution O 1s spectrum is presented in Fig. 4b. The O 1s XPS spectrum of sample is illustrated in Fig. 4b, which can be deconvoluted as three peaks. The peaks at 532.8 and 530.3 eV are ascribed to O 1s of H_2O and O^{2-}, respectively, while the peak at 531.6 eV is assigned to C–O, C=O and COO bonds [34]. The presence of three different oxygen species observed in the O1s spectrum indicates that the surface is oxygen enriched.. The XPS results also confirm the formation of α-Fe_2O_3, which is in good agreement with the XRD result. TEM image of the products is presented in Fig. 4c. It shows that the product consists of nanoparticles with an average size of about 20 nm and has a porous structure. The nitrogen adsorption/desorption isotherms is presented in Fig. 4d. The physisorption measurement is essentially the type IV isotherm with H2-type hysteresis loops associated with the capillary and wormhole-like pores [35]. Such hysteresis typically indicates the presence of mesopores, according to the International Union of Pure and Applied Chemistry (IUPAC) [36]. A large hysteresis loop between the adsorption and desorption isotherms over the relative pressure, P/P_0, range of 0.45-0.98 is characteristic of highly porous materials, which confirmed the formation of mesopores in the flaky structure.

3.2. Optical properties and photocatalytic activity

Since high SSA mesoporous nanocrystalline α-Fe_2O_3 was synthesized at $\phi=0.3$, it was chosen for photocatalytic experiments. Optical absorption properties could reveal the spectrum range where light is being absorbed to excite the electrons in the catalyst [37]. The optical properties of the product were investigated by the UV–vis absorption spectra at room temperature. As shown in Fig. 5a, the α-Fe_2O_3 has strong photo absorption in the UV and visible spectral regions, and the wavelength of the absorption edge is 640 nm. According to the equation $\alpha E_p=K(E_p-E_g)^{1/2}$ (where α is the adsorption coefficient, K is a constant, E_p is the discrete photo energy, and E_g is the band gap energy), a classical Tauc approach was further employed to estimate the E_g value of the α-Fe_2O_3 nanocrystals [38,39]. A plot of $(\alpha E_p)^2$ versus E_p, based on the direct transition, is shown as the inset image in Fig. 5a. The extrapolated value of E_p at=0 gives absorption edge energies' correspondence to $E_g=2.03$ eV, which is corresponding with the reported value ($E_g=1.9$-2.2 eV).

To investigate α-Fe_2O_3 visible light photocatalytic performance for degradation of organic pollutants, methylene blue was selected as a model contaminant for photocatalytic decolorization. Fig. 5b shows the changes in the absorption spectra of the MB aqueous solution exposed to visible light over time in the presence of the products. The MB spectrum reveals a major absorption band at 664 nm. The characteristic absorption peak of MB molecules at 664 nm rapidly decreased in intensity with time and disappeared completely after about 100 min. These results indicate that the synthesized mesporous α-Fe_2O_3 crystalline is a promising catalyst for the removal of organic pollutants.

Fig. 6 shows the comparison of photocatalytic activity of the samples prepared at different conditions. In the absence of

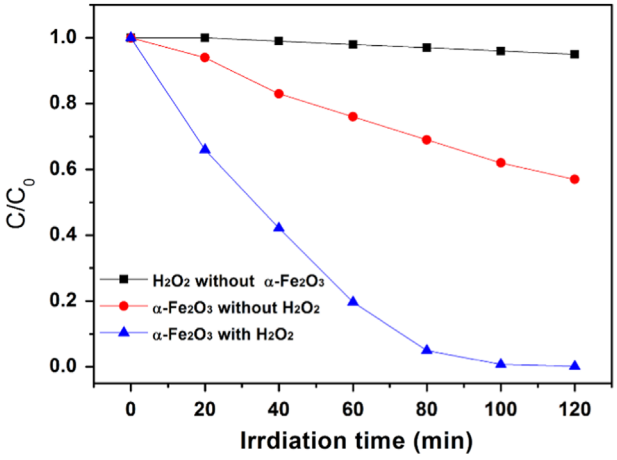

Fig. 6. Comparison of the photocatalytic activity for MB with different conditions: (■) H_2O_2 without α-Fe_2O_3, (●) α-Fe_2O_3 without H_2O_2, (▲) α-Fe_2O_3 with H_2O_2.

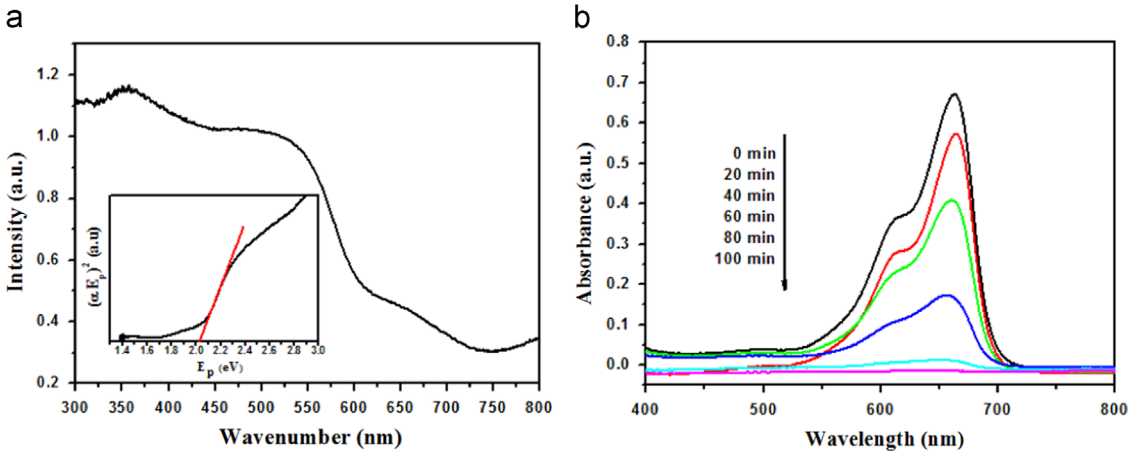

Fig. 5. (a) Optical absorption spectrum of the α-Fe_2O_3 particles (inset, plot of the square of absorbance versus photon energy); (b) Changes of the time-dependent UV–vis absorbance spectra in the presence of α-Fe_2O_3 sponge under visible light irradiation for different amount of time.

α-Fe_2O_3, H_2O_2 shows almost no photocatalytic activity under visible light illumination for the decolorization of the MB aqueous solution. In the absence of H_2O_2, the prepared α-Fe_2O_3 particles show weak photocatalytic activity under visible light illumination. However, in the presence of H_2O_2 under visible-light illumination, the prepared α-Fe_2O_3 particles obviously show visible light photocatalytic activity. It is known that H_2O_2 addition enhances the rate of dye photodegradation, ascribed to the combined effects of the conduction electron scavenging and the Fenton reaction [40]. The Fenton reaction is one of the most effective advanced oxidation processes for waste water treatment, which is well-known as the production of hydroxyl radicals ($\cdot$OH) by reaction between Fe^{2+} and H_2O_2 [41]. The formation of $\cdot$OH triggers the photocatalytic reaction. The results in this work also confirm this theory.

4. Conclusion

The highly mesoporous α-Fe_2O_3 is synthesized by solution combustion synthesis under fuel-lean conditions in one step, simply by selecting a proper fuel to oxidizer ratio, ϕ. The α-Fe_2O_3 consists of nanoparticles with an average size of about 20 nm. The hematite displays a continuous absorption band in the visible region and the photocatalytic activity is evaluated by degrading the methylene blue pollutant in water at ambient temperature. The synthesized mesoporous hematite is a promising visible light photocatalyst for organics decomposition.

Acknowledgements

This work was supported by the National Natural Science Foundation Program of China (50802006) and (51172017), the Program for the New Century Excellent Talents in University (NCET-10-0226), and the Fundamental Research Funds for the Central Universities (FRF-TP-11-004A) and the National 863 Program (2013AA031101).

References

[1] J. Luo, M. Lin, T. He, C.F. Ng, S. Wang, H. Sun, H.J. Fan, TiO2/(CdS, CdSe, CdSeS) nanorod heterostructures and photoelectrochemical properties, J Phys Chem C 116 (2012) 11956–11963.
[2] Y. Ling, G. Wang, D.A. Wheeler, J.Z. Zhang, Y. Li, Sn-doped hematite nanostructures for photoelectrochemical water splitting, Nano Lett 11 (2011) 2119–2125.
[3] M. Muruganandham, R. Amutha, M. Sathish, T.S. Singh, R.P.S. Suri, M. Sillanp, Facile fabrication of hierarchical α-Fe2O3: self-assembly and its magnetic and electrochemical properties, J Phys Chem C 115 (2011) 18164–18173.
[4] X. Gou, G. Wang, J. Park, H. Liu, J. Yang, Monodisperse hematite porous nanospheres: synthesis, characterization, and applications for gas sensors, Nanotechnology 19 (2008) 125606.
[5] D. Bi, Y. Xu, Improved photocatalytic activity of WO3 through clustered Fe2O3 for organic degradation in the presence of H2O2, Langmuir 27 (2011) 9359–9366.
[6] J.G. Yu, X.X. Yu, B.B. Huang, X.Y. Zhang, Y. Dai, Hydrothermal synthesis and visible-light photocatalytic activity of novel cage-like ferric oxide hollow spheres, Cryst. Growth Des 9 (2009) 1474–1480.
[7] S.-Y. Sina, K.G.U. Wijayantha, A.A. Tahir, B. Vaidhyanathan, Nanostructured α-Fe2O3 electrodes for solar driven water splitting: effect of doping agents on preparation and performance, J. Phys. Chem. C 113 (2009) 4768–4778.
[8] M. Zhang, Y. Lin, T.J. Mullen, W.-F. Lin, L.-D. Sun, C.-H. Yan, T.E. Patten, D. Wang, G. Liu, Improving hematite's solar water splitting efficiency by incorporating rare-earth upconversion nanomaterials, J. Phys. Chem. Lett 3 (2012) 3188–3192.
[9] L. Xi, P.S. Bassi, S.Y. Chiam, W.F. Mak, P.D. Tran, J. Baber, Surface treatment of hematite photoanodes with zinc acetate for water oxidation, Nanoscale 4 (2012) 4430–4433.
[10] K. Sivula, F.L. Formal and M. Gratzel, water splitting: progress using hematite α-Fe2O3 photoelectrodes, Chem. Sus. Chem 4 (2011) 432–449.
[11] M. Zhu, Y. Wang, D. Meng, X. Qin, G. Diao, Hydrothermal synthesis of hematite nanoparticles and their electrochemical properties, J. Phys. Chem. C 116 (2012) 16276–16285.
[12] B. Klahr, S. Gimenez, F. Fabregat-Santiago, T. Hamann, J. Bisquert, Water oxidation at hematite photoelectrodes: the role of surface states, J. Am. Chem. Soc. 134 (2012) 4294–4302.
[13] J.D. Atkinson, M.E. Fortunato, S.A. Dastgheib, M. Rostam-Abadi, M.J. Rood, K.S. Suslick, Synthesis and characterization of iron-impregnated porous carbon spheres prepared by ultrasonic spray pyrolysis, Carbon 49 (2011) 587–598.
[14] S. Bharathi, D. Nataraj, D. Mangalaraj, Y. Masuda, K. Senthil, K. Yong, Highly mesoporous α-Fe2O3 nanostructures: preparation, characterization and improved photocatalytic performance towards Rhodamine B (RhB), J. Phys. D: Appl. Phys 43 (2010) 015501.
[15] Y. Ren, A.R. Armstrong, F. Jiao, P.G. Bruce, Influence of size on the rate of mesoporous electrodes for lithium batteries, J. Am. Chem. Soc. 132 (2010) 996–1004.
[16] IUPAC Manual of Symbols and Terminology, Appendix 2, Part 1, Colloid and Surface Chemistry, Pure Appl. Chem. 31 (1972) 578.
[17] A.S. Prakash, P. Manikandan, K. Ramesha, M. Sathiya, J.-M. Tarascon, A.K. Shukla, Solution-combustion synthesized nanocrystalline Li4Ti5O12 as high-rate performance Li-ion battery anode, Chem. Mater. 22 (2010) 2857–2863.
[18] P.A. Deshpande, S. Polisetti, G. Madras, Solution-combustion synthesized nanocrystalline Li4Ti5O12 as high-rate performance Li-ion battery anode, Langmuir 27 (2011) 3578–3587.
[19] M. Mapa, C.S. Gopinath, Combustion synthesis of triangular and multifunctional $ZnO1-xNx$ ($x \leq 0.15$) materials, Chem. Mater. 21 (2009) 351–359.
[20] S.T. Aruna, N.S. Kini, N.S. Rajam, Solution combustion synthesis of CeO2–CeAlO3 nano-composites by mixture-of-fuels approach, Mater. Res. Bull. 44 (2009) 728–733.
[21] S.L. González-Cortés, F.E. Imbert, Fundamentals, properties and applications of solid catalysts prepared by solution combustion synthesis (SCS), Applied Catalysis A: General 452 (2013) 117–131.
[22] J. Toniolo, A.S. Takimi, M.J. Andrade, R. Bonadiman, C.P. Bergmann, Synthesis by the solution combustion process and magnetic properties of iron oxide (Fe3O4 and α-Fe2O3) particles, J. Mater. Sci. 42 (2007) 4785–4791.
[23] K. Deshpande, M. Nersesyan, A. Mukasyan, A. Varma, Novel ferromagnetic iron oxide nanopowders, Ind. Eng. Chem. Res. 44 (2005) 6196–6199.
[24] P. Hu, S. Zhang, H. Wang, D. Pan, J. Tian, Z. Tang, A.A. Volinsky, Heat treatment effects on Fe3O4 nanoparticles structure and magnetic properties prepared by carbothermal reduction, J. Alloys Compd 509 (2011) 2316–2319.
[25] P. Erri, J. Nader, A. Varma, Controlling combustion wave propagation for transition metal/alloy/cermet foam synthesis, Adv. Mater. 20 (2008) 1243–1245.
[26] K. Deshpande, A. Mukasyan, A. Varma, Direct synthesis of iron oxide nanopowders by the combustion approach: reaction mechanism and properties, Chem. Mater. 16 (2004) 4896–4904.
[27] C.-H. Jung, S. Jalota, S.B. Bhaduri, Quantitative effects of fuel on the synthesis of Ni/NiO particles using a microwave-induced solution combustion synthesis in air atmosphere, Mater. Lett. 59 (2005) 2426–2432.

[28] S.S. Manoharan, S.J. Swati, M.L. Prasanna, Rao, R.K. Sahu, Microwave-assisted synthesis of fine particle oxides employing wet redox mixtures, J. Am. Ceram. Soc. 85 (2002) 2469–2471.
[29] B. Zhao, X. Yu, R. Cai, R. Ran, H. Wang, Z. Shao, Solution combustion synthesis of high-rate performance carbon-coated lithium iron phosphate from inexpensive iron (III) raw material, J. Mater. Chem. 22 (2012) 2900–2907.
[30] D.A. Fumo, M.R. Morelli, A.M. Segadaes, Combustion synthesis of calcium aluminates, Mater. Res. Bull. 31 (1996) 1243–1255.
[31] J. Bai, J. Liu, C. Li, G. Li, Q. Du, Mixture of fuels approach for solution combustion synthesis of nanoscale MgAl2O4 powders, Adv. Powder Technol. 22 (2011) 72–76.
[32] I. Ganesh, B. Srinivas, R. Johnson, B.P. Saha, Y.R. Mahajan, Effect of fuel type on morphology and reactivity of combustion synthesised MgAl2O4 powders, Br. Ceram. Trans 101 (2002) 247–254.
[33] D. Patil, V. Patil, P. Patil, Highly sensitive and selective LPG sensor based on α-Fe2O3 nanorods, Sens Actuators B 152 (2011) 299–306.
[34] A. Jitianu, T. Cacciaguerra, R. Benoit, S. Delpeux, F. B´eguin, S. Bonnamy, Synthesis and characterization of carbon nanotubes–TiO2 nanocomposites, Carbon 42 (2004) 1147–1151.
[35] B.Y. Yu, S.-Y. Kwak, Carbon quantum dots embedded with mesoporous hematite nanospheres as efficient visible light-active photocatalysts, J. Mater. Chem. 22 (2012) 8345–8353.
[36] S. Lowell, J.E. Shields, M.A. Thomas, M. Thommes and M. Kluwer, Academic Publishers, Boston, (2004) 101–126 4th edn.
[37] J.H. Ye, J.W. Tang, Z.G. Zou, Efficient photocatalytic decomposition of organic contaminants over CaBi2O4 under visible-light irradiation, Angew. Chem. Int. Ed. 43 (2004) 4463–4466.
[38] B. Jia, M. Qin, X. Jiang, Z. Zhang, L. Zhang, Y. Liu, X. Qu, Synthesis, characterization, shape evolution, and optical properties of copper sulfide hexagonal bifrustum nanocrystals, J. Nanopart. Res. 15 (2013) 1469.
[39] D.R. Cummins, H.B. Russell, J.B. Jasinski, M. Menon, K.M. Sunkara, Iron Sulfide (FeS) nanotubes using sulfurization of hematite nanowires, Nano. Lett. 13 (2013) 2423–2430.
[40] T. Sugimoto, Y. Wang, H. Itoh, A. Muramatsu, Systematic control of size, shape and internal structure of monodisperse α-Fe2O3 particles, Colloids Surf. A 134 (1998) 265–279.
[41] Y.G. Zhang, L.L. Ma, J.L. Li, Y. Yu, In situ Fenton reagent generated from TiO2/Cu2O composite film: a new way to utilize TiO2 under visible light irradiation, Environ. Sci. Technol. 41 (2007) 6264–6269.